Supplementary Information: Remote Focused Encoding and Decoding of Electric Fields through Acoustoelectric Heterodyning

Jean L. Rintoul[1], Esra Neufeld[2], Chris Butler[1], Robin O. Cleveland[3], Nir Grossman[1]

[1]Department of Brain Sciences, Imperial College London, London, UK. [2]Foundation for Research on Information Technologies in Society (IT'IS), Zurich, Switzerland. [3]Institute of Biomedical Engineering, University of Oxford, Oxford, UK

Correspondence to: jeanrintoul@imperial.ac.uk; nirg@imperial.ac.uk

Supplementary Note 1. Mathematical model of acoustoelectric field generation in electrolytic liquids and soft tissues

a. Detailed derivation of the mathematical model of the electrolytic acoustoelectric effect

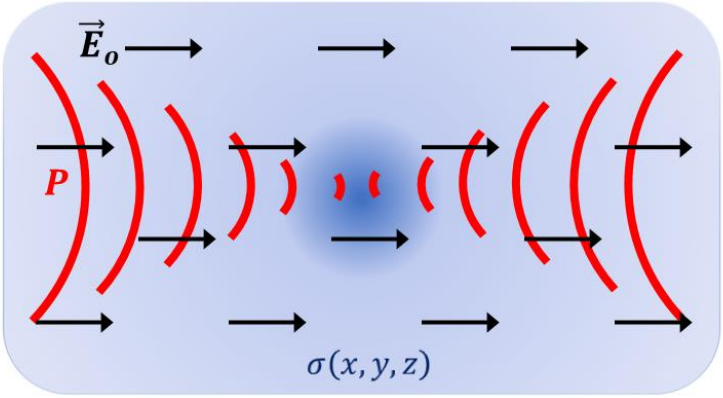

Supplementary Figure 1| Model schematic.

We assume an external electric field $\vec{E}_o(x,y,z)$ that induces ionic currents with a density $\vec{J}(x,y,z)$ in an electrolytic liquid (or soft tissue) with a conductivity distribution $\sigma(x,y,z)$, **Supplementary Figure 1**. According to Gauss's theory, the integral of the normal component of the current vectors over a closed surface is equal to the integral of the current source density within the enclosed volume[1]. Thus, if the current source is external to the volume of interest, the divergence of the current density is zero at any location within the volume of interest.

$$\nabla \cdot \vec{J} = 0 \qquad (1)$$

According to Ohm's law, the current density equals to the product of the electric field and conductivity[1].

$$\vec{J} = \sigma \vec{E}_o \qquad (2)$$

Combining **Eq. 1** and **2** states that the divergence of the product of the conductivity and electric field is zero within the volume of interest.

$$\nabla \cdot \left(\sigma \vec{E}_o\right) = 0 \qquad (3)$$

If an acoustic pressure field $P(x,y,z)$ is concurrently applied to the electrolytic medium, it creates a conductivity perturbation $\sigma_{ae}(x,y,z)$ due to the electrolyte's compression and rarefaction in space and the associated changes in ion concentration. This conductivity perturbation creates an electric field modulation $\vec{E}_{ae}$ such that Gauss's law of net-zero flux is again satisfied.

$$\nabla \cdot \left((\sigma + \sigma_{ae})(\vec{E}_o + \vec{E}_{ae})\right) = 0 \qquad (4)$$

Expanding we get

$$\nabla \cdot (\sigma \vec{E}_0) + \nabla \cdot (\sigma \vec{E}_{ae}) + \nabla \cdot (\sigma_{ae} \vec{E}_0) + \nabla \cdot (\sigma_{ae} \vec{E}_{ae}) = 0 \qquad (5)$$

The first term equals zero due to **Eq. 3**, leaving

$$\nabla \cdot (\sigma \vec{E}_{ae}) + \nabla \cdot (\sigma_{ae} \vec{E}_0) + \nabla \cdot (\sigma_{ae} \vec{E}_{ae}) = 0 \qquad (6)$$

The last term is a product of two small quantities and can be neglected (see **Supplementary Note 1 b**). **Eq. 6** is then reduced to

$$\nabla \cdot (\sigma \vec{E}_{ae}) + \nabla \cdot (\sigma_{ae} \vec{E}_0) = 0 \quad (7)$$

The conductivity of electrolytic solutions is governed by the concentration and mobility of the dissolved ions. In an electrolyte, the conductivity can be expressed as

$$\sigma = F\gamma_{\pm} k_d c(z_+\mu_+ + z_-\mu_-) \quad (8)$$

where F is the Faraday constant, $\gamma_{\pm}$ is the mean activity coefficient, k_d is the dissociation constant, c is the solute molar concentration (i.e., molarity), z_+ and z_- are the charge number (i.e., valence) of the cation and anion, respectively, and μ_+ and μ_- are the electrical mobility of the cations and anions, respectively[2]. Physiological saline is considered in this study as a strong electrolyte with a low molar concentration of single valence ions resulting in $\gamma_{\pm}$ and k_d values of ~1. Thus, the conductivity is governed by the concentration and mobility of the dissolved ions. In saline $z_+ = z_- = 1$, and $\mu_+ \approx \mu_- = \mu$ hence

$$\sigma \approx 2Fc\mu \quad (9)$$

The partial derivative of conductivity in terms of molar concentration and mobility results in a relative change in conductivity proportional to the sum of the relative change in molar concentration and relative change in mobility

$$\frac{\partial \sigma}{\sigma} = \left(\frac{\partial c}{c} + \frac{\partial \mu}{\mu}\right) \quad (10)$$

The relative change in molar concentration c is exerted by the pressure induced compression and rarefaction of the solution's volume (V) with fixed number of ions. Under adiabatic conditions, the relative volume change is related to the pressure P by

$$\frac{dV}{V} = -\beta P \quad (11)$$

where β is the medium's adiabatic compressibility. Since

$$c = \frac{n}{V} \quad (12)$$

where n is the ions amount in moles, the derivative of the molar concentration in terms of volume results in a relative change in molar concentration equal to the product of the pressure P and the medium's adiabatic compressibility β.

$$\frac{\partial c}{c} = \beta P \quad (13)$$

The relative change in mobility μ is exerted via the pressure-induced change to the solution's temperature and viscosity[3] controlled by Van der Waals interactions. The change in viscosity is negatively proportional to the pressure at temperatures higher than 4°C[4]. The change in temperature is positively proportional to the pressure via the medium's volumetric (cubic) thermal expansion coefficient[5]. Thus

$$\frac{\partial \mu}{\mu} = \alpha P \quad (14)$$

were α is a constant.

As a result, the relative change in conductivity is proportional to the applied pressure

$$\frac{\partial \sigma}{\sigma} = (\beta + \alpha)P = kP \tag{15}$$

were k is a constant incorporating the pressure dependent changes in relative molar concentration and ionic mobility.

Substituting **Eq. 15** into **Eq. 7**

$$\nabla \cdot \left(\sigma \, \vec{E}_{ae}\right) + \nabla \cdot \left(\sigma k P \, \vec{E}_0\right) = 0 \tag{16}$$

Using the divergence product rule ($\nabla \cdot \left(a\vec{b}\right) = a(\nabla \cdot \vec{b}) + \nabla a \cdot \vec{b}$) we get

$$\nabla \cdot \left(\sigma \vec{E}_{ae}\right) + \nabla(kP) \cdot \left(\sigma \vec{E}_0\right) + kP \nabla \cdot \left(\sigma \vec{E}_0\right) = 0 \tag{17}$$

Since $\nabla \cdot \left(\sigma \vec{E}_0\right) = 0$ in **Eq. 7**, we get

$$\nabla \cdot \left(\sigma \vec{E}_{ae}\right) = -\nabla(kP) \cdot (\sigma \vec{E}_0) \tag{18}$$

It can be seen that the amplitude of the resultant acoustoelectric effect depends on the relative orientation of the pressure gradient to the electric field.

Special Case 1. Homogeneous medium

If the region of interest has a constant adiabatic compressibility and conductivity we get

$$\nabla \cdot \vec{E}_{ae} = -k \nabla P \cdot \vec{E}_0 \tag{19}$$

Special Case 2. Infinite planar transducer

In the case of an ideal infinite planar transducer, pressure travels in one direction, and if the electric field is oriented in the same direction, or shows the same translational symmetry, the acoustoelectric model can be reduced to a scalar one. In cartesian coordinates, **Eq. 19** can be written as

$$\frac{\partial E_{ae,x}}{\partial x} + \frac{\partial E_{ae,y}}{\partial y} + \frac{\partial E_{ae,z}}{\partial z} = -k \frac{\partial P}{\partial x} \mathrm{E}_{0,x} - k \frac{\partial P}{\partial y} \mathrm{E}_{0,y} - k \frac{\partial P}{\partial z} \mathrm{E}_{0,z} \tag{20}$$

where $E_{ae,j}$ and $\mathrm{E}_{o=0,j}$ are the component of the generated acoustoelectric field and applied electric field in the $\hat{j}$ direction ($\hat{j} = \hat{x}, \hat{y}, \hat{z}$), respectively. If the acoustic field is applied via an infinite planar transducer and the electric field is parallel to the acoustic field propagation (or shows the same $\hat{y}\hat{z}$ translational symmetry)

$$\frac{dE_{ae,y}}{dy} = \frac{dE_{ae,z}}{dz} = k \frac{dP}{dy} \mathrm{E}_{0,y} = k \frac{dP}{dz} \mathrm{E}_{0,z} = 0 \tag{21}$$

Thus, we get a one-dimensional equation

$$\frac{dE_{ae}(x)}{dx} = -k \frac{dP(x)}{dx} \mathrm{E}_0(x) \tag{22}$$

Integrating over x, using the integration by parts rule ($\int f'g = fg - \int fg'$)

$$E_{ae}(x) = -kP(x)\mathrm{E}_0(x) + k\int_0^x P(x)\frac{d\mathrm{E}_0(x)}{dx}dx + c \qquad (23)$$

The constant c must be zero because there is no E_{ae} without E_0 and P. If the electric field is homogenous such that $\frac{dE_0(x)}{dx} = 0$, we get:

$$E_{ae} = -kP\mathrm{E}_0 \qquad (24)$$

The amplitude of the acoustoelectric field under these special exposure conditions is proportional to the multiplication of the pressure and the background electric field. This equation thus reduces to the commonly employed equation[6], which is revealed to be a special case of a more general model.

b. Small Term Assumption

We aim to compare the magnitude of $\nabla\cdot\left(\sigma\vec{E}_{ae}\right)$ and $\nabla\cdot\left(\sigma_{ae}\vec{E}_0\right)$ with that of $\nabla\cdot\left(\sigma_{ae}\vec{E}_{ae}\right)$ in **Eq. 6**. σ_{ae} is smaller than σ by a factor kP, and based on **Eq. 17**, so is $\vec{E}_{ae}$ compared to $\vec{E}_0$.

However, a careful comparison also must consider that the product of $\sigma_{ae}\vec{E}_{ae}$ is the product of two distributions that both contain frequency components with spatial frequencies of $2\pi cf$, where c is the acoustic velocity in the medium of interest and f is the frequency. Thus $\sigma_{ae}\vec{E}_{ae}$ contains spatial frequencies up to twice that spatial frequency (multiplication in direct space corresponds to convolution in Fourier space), which leads to an additional factor of up to 2 when applying the gradient. As a result, the magnitude of $\nabla\cdot\left(\sigma_{ae}\vec{E}_{ae}\right)$ is in the order of $2kP$ smaller than that of $\nabla\cdot\left(\sigma\vec{E}_{ae}\right)$ and $\nabla\cdot\left(\sigma_{ae}\vec{E}_0\right)$.

Assuming the acoustic change in conductivity is based on the change in molar concentration and ionic mobility[7,8] i.e., $k = 1\mathrm{x}10^{-9}[1/Pa]$ and that the peak pressure is in the order of $10^6[Pa]$, $2kP = 0.002 \ll 1$, thus confirming **Eq. 6** is at least a self-consistent approximation.

Supplementary Note 2. Characterization of the applied and generated fields in the computational model

The gradient of the pressure field, i.e., force density, affects the generated electric field. The components of this pressure-based vector are shown in **Supplementary Figure 2a-b**. In the radial plane (i.e., perpendicular to the acoustic field propagation), the force density changes direction periodically in a concentric ring's geometry while in the axial plane, the force density changes direction periodically on a wavelength scale governing the shape of the acoustoelectrically generated electric field see in **Fig. 1**. The components of the acoustoelectrically generated electric field the x,y,z orientations are governed by the product between the applied force density and electric field in those orientations. Although force density may be well understood in classical mechanics, considering it as a source of electromagnetic oscillation is unexplored.

The frequency mixing property of the acoustoelectric effect results in generated electric fields that oscillate at the sum and difference frequencies. Hence, the temporal spatial pattern of the combined fields depends on the frequencies of the applied fields. **Supplementary Figure 2c** shows example time evolutions of the generated field for different applied frequencies. The spatial distribution changes dependent on the relative phase difference between the sum and difference frequencies.

Supplementary Figure 2d shows the relationship between the amplitude of the applied electric and acoustic fields and the amplitude of the generated electric field when the applied fields are parallel, demonstrating a linear relationship between the generated electric field amplitude and the applied electric field amplitude, consistent with previous studies[7]. Similarly, it shows a linear relationship between the generated electric field amplitude and the applied acoustic field amplitude, consistent with previous studies[9].

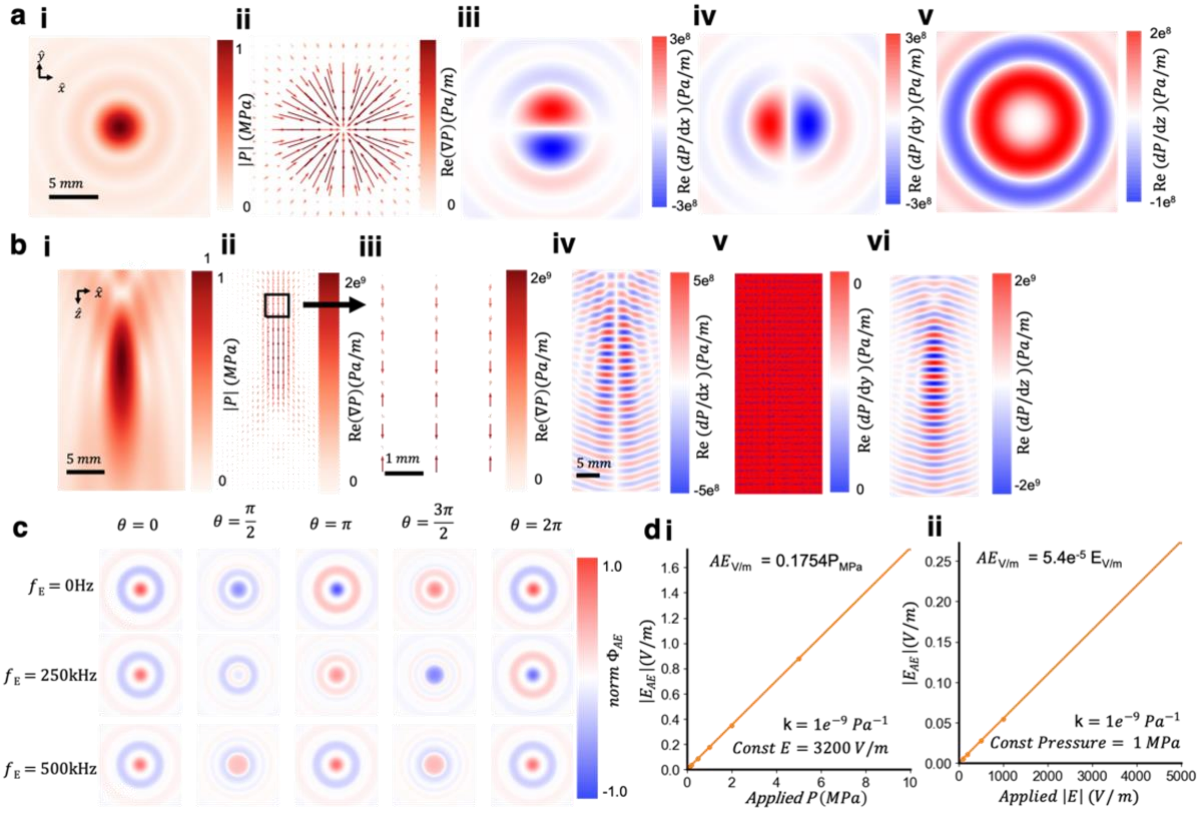

Supplementary Figure 2 | Characterisitics of the applied acoustic fields & acoustoelectrically generated electric field obtained through computational modeling (related to Fig. 1).

a, Acoustic pressure distribution in the radial plane $\hat{x}\hat{y}$ of the ultrasound transducer with f_A=500 kHz and peak amplitude 1 MPa propagating in the $\hat{z}$ direction. (**i**) Map of pressure amplitude. (**ii**) Vector map of pressure gradient. (**iii**), Map of $\hat{x}$ component of the pressure gradient. (**iv**) same as (iii) but $\hat{y}$ component. (**v**) same as (iii) but $\hat{z}$ component. **b**, Same as (a) but in the axial plane $\hat{x}\hat{z}$. **c**, Evolution of the acoustoelectrically generated electric field via focal acoustic field as in (a) and a homogeneous electric field of 3.2kV/m parallel to the propagation of the acoustic field propagation. Shown are normalized Φ_{AE} maps in the radial plane $\hat{x}\hat{y}$ at different instantaneous phase θ of the ultrasound transducer period ($^1/_{f_A}$). **d**, Peak amplitude of the acoustoelectrically generated electric fields versus (**i**) peak amplitude of applied acoustic field with applied electric field amplitude fixed (here at 3.2kV/m), (**ii**) amplitude of applied electric field with fixed acoustic field amplitude (here at 1 MPa at the peak); electric field was parallel to the propagation of the acoustic field propagation.

Supplementary Note 3. Characterization of the applied and measured fields in the saline measurements

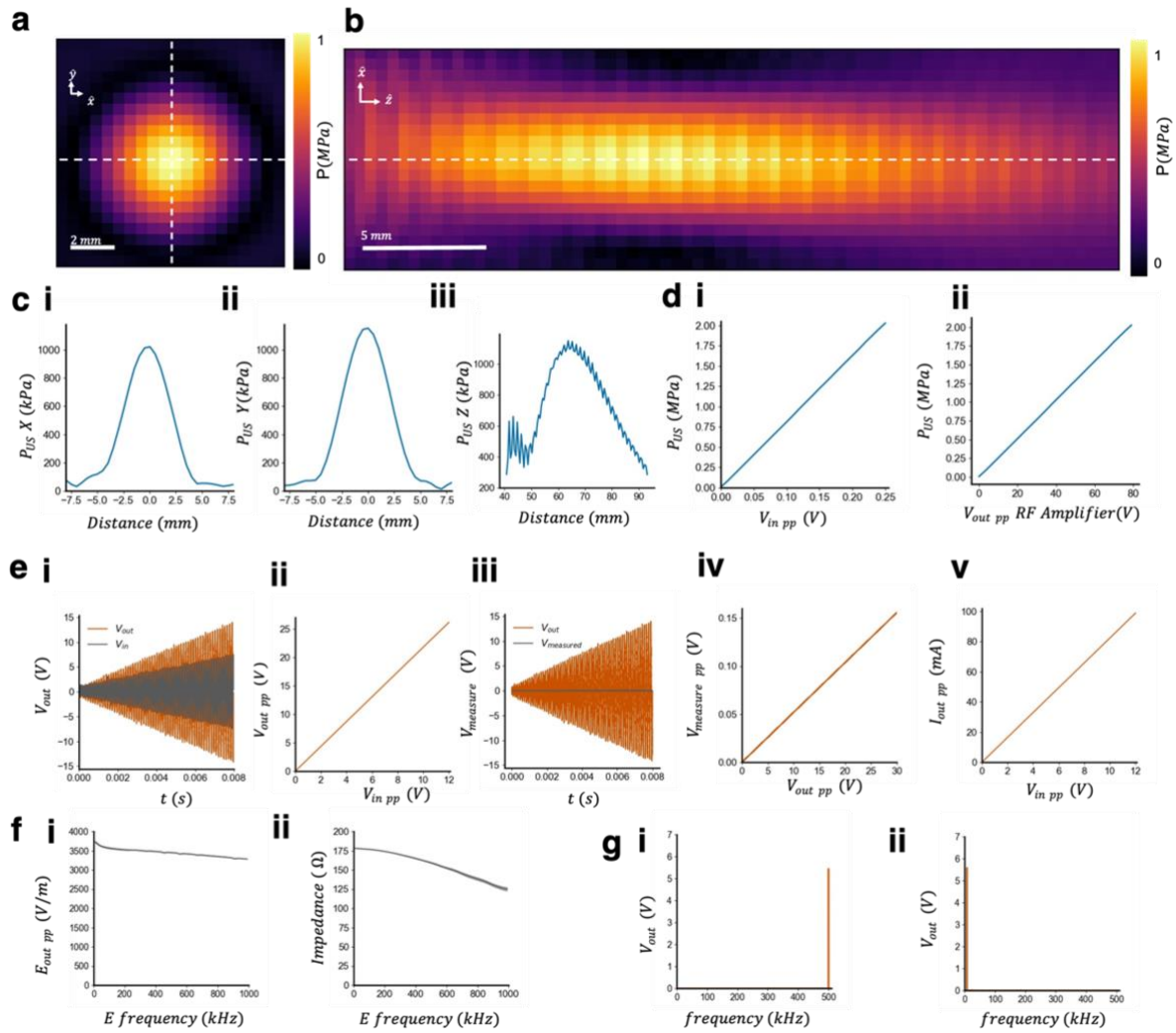

Supplementary Figure 3 | Characterization of the applied acoustic and electric fields (related to Fig. 2-4).

a-**d**, Characterization of the applied acoustic field. **a**, Map of acoustic pressure amplitude in the radial plane $\hat{x}\hat{y}$ (left), i.e., perpendicular to the acoustic field propagation direction, measured with 0.2 mm hydrophone (sensitivity = 52 mV/MPa). **b**, Same as in (a) but in the axial plane $\hat{x}\hat{z}$, i.e., parallel to the acoustic field propagation. **c,** Line plot of the measured acoustic pressure amplitude along the (**i**) $\hat{x}$ direction, (**ii**) $\hat{y}$ direction, and (**iii**) $\hat{z}$ direction. Note, the recording in the $\hat{z}$ direction (i.e., axial) shows small standing waves effect, despite the damping material at the back of tank potentially due to the long recording period (8 ms). **d,** Measured acoustic pressure amplitude vs amplitude of the driving voltage to the ultrasound transducer (**i**) before the RF amplifier (**ii**) after the RF amplifier. **e**-**f**, Characterization of the applied electric field. **e**, Electric voltage output. (**i**), Ramped sine wave used to characterize the electric field generated in saline via the platinum iridium electrode probe. (**ii**), Relationship between the function generator voltage (V_{in}) and the output of the voltage source (V_{out}), i.e., the isolation transformer with x2 gain; shown values are peak-to-peak (pp) amplitudes. (**iii**), Amplitude ramp function delivered to saline showing output of isolation transformer and measured electric potential in the solution. (**iv**), Measured output of isolation transformer vs. voltage at the measurement electrodes; shown values are pp amplitudes. (**v**), Output current amplitude, measured across a resistor in series vs. measured function generator output voltage; shown values are pp amplitudes. **f**, Electric field output. (**i**) Applied electric field measured across the stimulation electrodes (3 mm spacing) in saline vs applied frequency. (**ii**) Computed impedance across the stimulation electrodes vs. applied frequency. **g**, Measured amplitude spectra of (**i**) acoustic field when a 500 kHz pressure was applied, (**ii**) electric field when a 8 kHz electric field was applied.

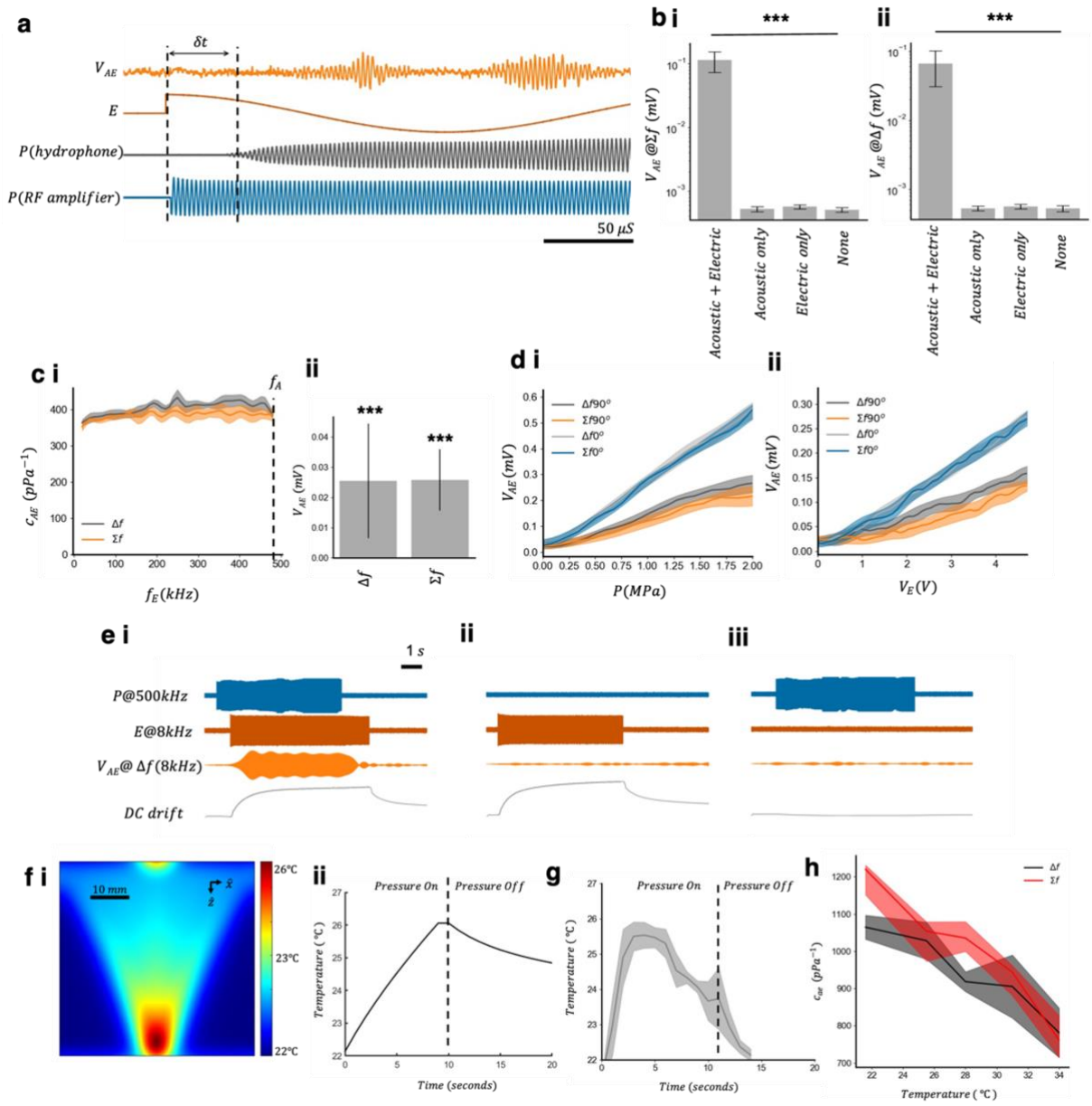

Supplementary Figure 4 | Characteristics of the acoustoelectrically generated electric fields (related to Fig. 2-4).

a, Zoomed view of the onset of the acoustoelectrically generated electric potential, showing the traces of the applied RF amplifier input to the ultrasound transducer (blue), resulting acoustic field at the phantom's measurement region (grey) as measured by hydrophone, applied electric field (red), generated acoustoelectric potential (orange). The onset of acoustoelectric generated fields mixing occurs after the hydrophone measurement of the arriving ultrasonic field. Here the frequencies of the applied acoustic and electric fields are as in **Fig. 3**. **b**, Amplitude of recorded V_{AE} at (**i**) the sum frequency $\sum f$, (**ii**) the difference frequency Δf under the same conditions as in (**Fig 3 d**) but comparing when both electric and acoustic fields were applied, only acoustic field was applied, only electric field was applied, no fields were applied; values are mean ±st.d.; *** indicates $p<10^{-20}$; significance was tested with Tukey's honest significance test corrected for multiple comparisons, n=50 measurements. **c**, Effect of the applied electric field frequency. (**i**) Acoustoelectric coupling factor c_{ae} at $\sum f$ and Δf vs. applied electric field frequency f_E with applied acoustic frequency f_A fixed at 500 kHz, the acoustoelectric field amplitude is estimated by the amplitude of the ASD at the relevant frequency; (**ii**) mean ±st.d. recorded V_{AE} amplitude across the frequency range in (**i**). *** indicates $p<10^{-20}$; significance was tested with

pairwise t-test against the condition in which no fields were applied; n=200 measurements. **d,** Amplitude of the acoustoelectrically generated electric potential vs. (**i**) amplitude of the applied acoustic field with the amplitude of the applied electric field fixed (here at 3.2k V/m), (**ii**) amplitude of applied electric potential with the amplitude of the applied acoustic field fixed (here at 1 MPa at the peak). Shown are mean ±st.d. values at the difference frequency Δf and sum frequency $\sum f$ when the fields are parallel (0°) or perpendicular (90°); n= 50 measurements; light grey, 0°at Δf; blue, 0°at $\sum f$; dark grey, 90° at Δf; orange, 90° at $\sum f$; Here the acoustic field frequency f_A=500 kHz and electric field frequency f_E=8 kHz. **e**, Representative time-synced recordings of the applied acoustic field P (blue), applied electric field E (red), acoustoelectrically generated electric field (orange), and extraneous DC drift (grey) when (**i**) both the acoustic and electric fields were applied (**ii**) only the electric field was applied (**iii**) only the acoustic field was applied. **f-g**, Characterisation of pressure induced thermal increase. **f**, Simulation of thermal changes using k-wave[10]. **i,** Temperature map **ii,** Temperature dissipation over time at the ultrasound focus, with 10 second continuous pressure wave and maximum focal pressure 1 MPa **g,** Physiological phantom measurements of thermal changes at the ultrasound focus. **h**, Acoustoelectric coupling factor at focal region vs. the saline temperature as phantom is heated.

Supplementary Note 4. Instrumentation

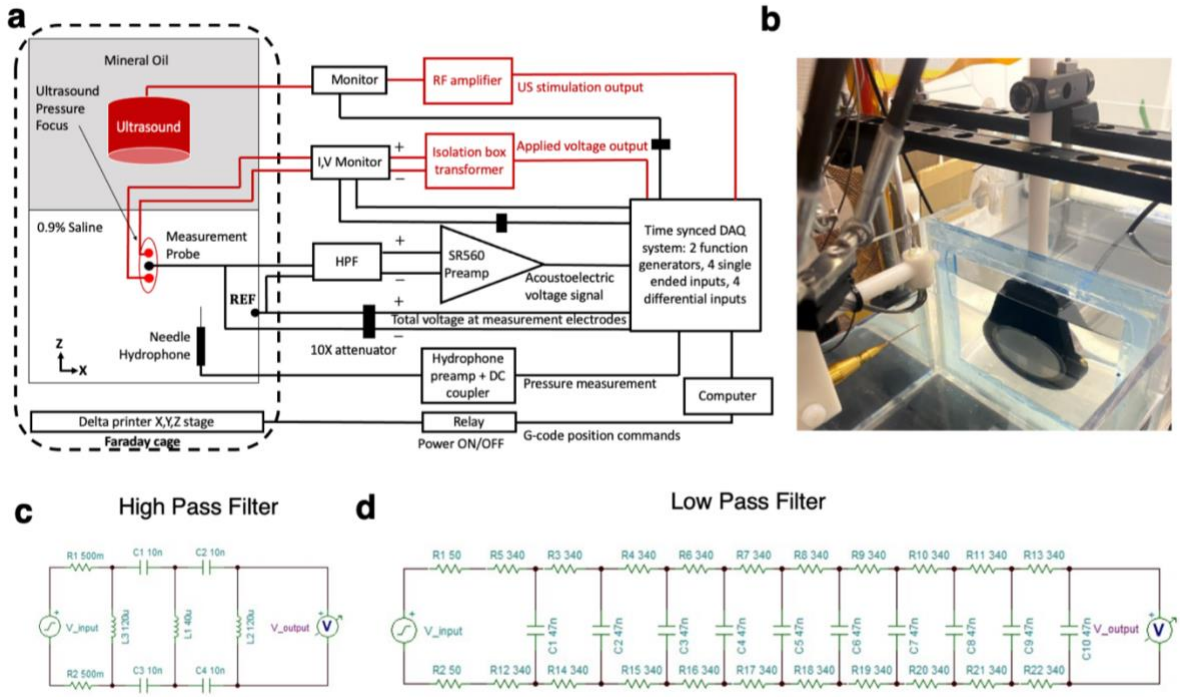

Supplementary Figure 5 | Instrumentation overview.

a, Schematic of instrumentation set up to enable monitoring of all signals while applying known pressures and electric fields. **b**, Image of the hydrophone and probe mounted into XYZ stage delta printer, with custom 3D printed probe[11], PDVF saline/mineral oil interface between transducer and measurement area. **c**, Electrical design for differential high-pass filter used in measurements. **d**, Electrical design of differential low-pass filter used in measurements in figures.

Supplementary Reference

1. I. S. Grant, W. R. P. Electromagnetism, 2nd Edition. 122–123 (1991).
2. Jossinet, J., Lavandier, B. & Cathignol, D. Impedance modulation by pulsed ultrasound. *Annals of the New York Academy of Sciences* vol. 873 396–407 Preprint at https://doi.org/10.1111/j.1749-6632.1999.tb09489.x (1999).
3. Lavandier, B., Jossinet, J. & Cathignol, D. Experimental measurement of the acousto-electric interaction signal in saline solution. *Ultrasonics* **38**, 929–936 (2000).
4. Partington, J. R. *Effect of pressure on the viscosity of liquids. In An Advanced Treatise on Physical Chemistry. Vol. 2, p. 89.* (Longmans, Green., 1955).
5. Pethig, R. Dielectric properties of biological materials: Biophysical and medical applications. *IEEE Transactions on Electrical Insulation* **EI-19**, 453–474 (1984).
6. Ragnar Olafsson, Russell S. Witte, Sheng-Wen Huang, M. O. Ultrasound Current Source Density Imaging. **55**, 1840–1848 (2008).
7. Li, Q., Olafsson, R., Ingram, P., Wang, Z. & Witte, R. Measuring the acoustoelectric interaction constant using ultrasound current source density imaging. *Phys Med Biol* **57**, 5929–5941 (2012).
8. Song, X., Qin, Y., Xu, Y., Ingram, P. & Witte, R. S. Tissue Acoustoelectric Effect Modeling From Solid Mechanics Theory. *IEEE Trans Ultrason Ferroelectr Freq Control* **64**, 1583–1590 (2017).
9. Yexian Qin, Zhaohui Wang, Pier Ingram, Qian Li, R. S. W. Optimizing Frequency and Pulse Shape for Ultrasound Current Source Density Imaging. *IEEE Trans Ultrasound Ferroelectrics and Frequency Control* **23**, 1–7 (2019).
10. Treeby, B. E. & Cox, B. T. k-Wave: MATLAB toolbox for the simulation and reconstruction of photoacoustic wave fields. *J Biomed Opt* **15**, 021314 (2010).
11. Ruiz-Vargas, A., Ivorra, A. & Arkwright, J. W. Design, Construction and Validation of an Electrical Impedance Probe with Contact Force and Temperature Sensors Suitable for in-vivo Measurements. *Scientific Reports* | **8**, (2018).